

# The Performance Evaluation of Static Obstacle Recognition by Underwater Pressure Characteristics for Underwater Spherical Robot

Ao Li<sup>1</sup>, Shuxiang Guo<sup>1,2,\*</sup>

1. The Key Laboratory of Convergence Biomedical Engineering System and Healthcare Technology, The Ministry of Industry and Information Technology, Beijing Institute of Technology, Beijing 100081, China

2. The Department of Electronic and Electrical Engineering, Southern University of Science and Technology, Shenzhen, Guangdong 518055, China

{ liao & guoshuxiang } @bit.edu.cn;

\* Corresponding author

**Abstract** - Underwater spherical robots are flexible and often perform tasks in narrow, dark and complex environments. The artificial lateral line system inspired by the lateral line system of fish can recognize obstacles. However, currently, the recognition of obstacles under the artificial lateral line system is mainly based on the vibration characteristics of obstacles. Based on the blank recognition of static obstacles, this paper analyzes the feasibility of recognition static obstacles. A polynomial regression model is proposed to detect static obstacles (walls) by moving robots. Finally, the effectiveness of obstacle recognition is verified by experiment and simulation.

**Index Terms** - Underwater pressure characteristics, Static obstacle recognition, Underwater spherical robot.

## I. INTRODUCTION

With the continuous development of science and technology, the exploitation of Marine resources becomes more and more important and urgent [1,2]. To explore the ocean, it is necessary to develop appropriate underwater exploration equipment and related technology. The positioning technology of underwater robot is the most critical underwater detection technology. How to accurately locate in the complex marine environment is an urgent problem to be solved. Currently, most autonomous underwater vehicles (AUVs) deploy radar, lasers and sonar to detect obstacles [3,4]. These detection methods have been shown to be effective under ideal environments. However, they do not work well under extreme environments, such as cramped, cloudy and dark spaces. In order to improve the stability and automation of AUVs in extreme environments, a new underwater positioning technology that is not affected by complex environments is needed.

Biological lateral line system has super sensitive flow sensing ability and can accurately perceive the flow disturbance around. Thus, by sensing of the lateral line system, fish carry out corresponding behaviors such as aggregation, rheology, and obstacle avoidance [5]. The lateral line system consists of hundreds of sensory units, which can be divided into two categories: Sympathetic Nervous System (SNs) and central nervous system (CNs). These features of the system have

inspired researchers to develop artificial lateral line systems (ALL). Artificial lateral line systems based on pressure or current velocity sensors have been developed over the past few decades. These systems are used to sense near-field hydrodynamic fluctuations and are applied for underwater target and current velocity detection. In addition, passive sensing is more popular than traditional detection technologies such as sonar when ecological conservation is considered.

The research of ALL system mainly focuses on ocean current and eddy current detection, attitude control and dipole positioning [6-8]. A large number of experiments have proved that ALLS can predict the current environments. Tuhtan et al. measured river ecosystems with ALLS. The results show that compared with traditional methods, ALLS has higher accuracy due to the reduction of measurement deviation and model dimension [6]. Xie et al. proposed a robotic box fish equipped with ALLS, which was used to detect Karman vortex street generated by tail fin oscillation of another robotic fish upstream. The relative vertical distance, relative yaw, pitch and roll angle between two adjacent robotic fish was obtained, and the attitude maintenance of the robot is realized. [7,8].

Target detection and recognition based on LLS sensor has been widely studied. Experimental and theoretical studies mostly use vibration or translational ball as stimulus. This is because, in practice, the location of some vibration targets can be simplified to the location of dipole sources. The flow field produced by dipole vibrations is approximately representative of the flow field produced by fins or insects, as well as the artificially swinging fins or propellers of underwater vehicles. Abdulsada et al. developed an ALL system with a sensor array for locating dipole sources in two-dimensional (2d) space [9]. Jiang et al. developed an ALLS that detects both pressure and velocity to locate the dipole [10]. Yang et al. proposed an ALL system consisting of 15 current velocity sensors placed laterally on a cylindrical platform for locating vibration sources in three-dimensional space [11]. Zheng et al. developed a cross-shaped ALL with 9 pressure sensors for 3D dipole positioning [12]. Xu et al. propose an improved distance evaluation method to evaluate the contribution of each sensor and discuss artificial lateral line systems optimization based on the optimal weight analysis algorithm [13].

In most studies on underwater target detection and location, such as dipole detection, bionic fish tail fin detection, cylindrical turbulence detection, etc., fluctuating water flow is generated by the target. However, in the real nature, there are still some stationary obstacles that do not produce water flow fluctuations. Avoiding these obstacles is very important in robot movement [14-17]. In addition, to obtain prediction models, most studies obtain flow field data through steady-state simulation. However, the movement of the robot is continuous. Therefore, dynamic simulation is necessary, and more data can be obtained at the same time. Moreover, the simulation data should stand up to experimental tests.

This paper analyzes the pressure characteristics of static obstacles (such as walls) around the robot during its movement. Data fitting was carried out by polynomial regression to evaluate the perception ability of the underwater vehicle to the fixed obstacles. The effectiveness of the proposed detection method is verified by experiments and numerical analysis. In this paper, a creative research is made on the recognition of stationary obstacles such as walls.

The rest of this article is organized as follows. The section II introduces the experimental platform and sensing algorithm are proposed in section III. In the section IV, the experimental results and discussion of wall surface localization are introduced. A summary of the concluding remarks is contained in section V.

## II. EXPERIMENTAL PLATFORM

### A. Platform Description

Experiments and verification of the robot were carried out through our experimental platform. The experimental platform consists of a bionic amphibious robot and movable sliding rail system. The bionic amphibious robot, shown in Fig. 1, is similar in shape to a turtle and consists of a hemispherical body and four legs. The hemispherical body contains the robot's circuitry and control systems. The four legs are flexible and driven by propellers. The robot weighs 6.6kg.

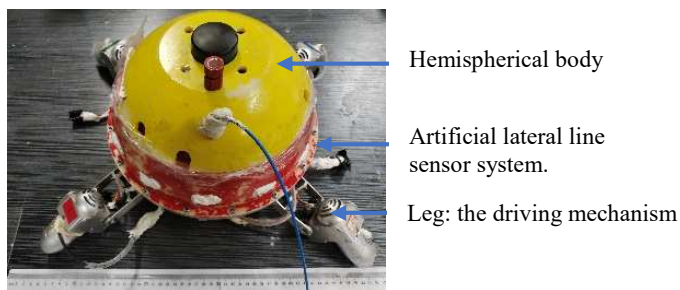


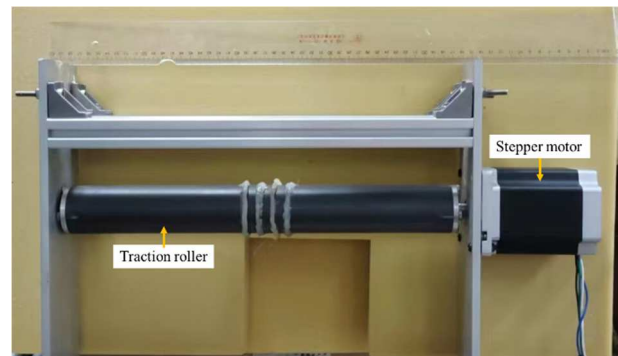
Fig. 1 The bionic amphibious robot equipped with artificial lateral line sensor system.

The movable sliding rail system consists of sliding rail, bracket, and stepper motor drive system. The length of the slide rail is 2 meters, and the sliding bracket is fixed on it. The robot is fixed on the sliding bracket and is drawn by the stepper motor to carry out uniform motion, as shown in Fig. 2 (a). The motor drive system consists of stepper motor, driver, controller, and switching power supply. The drive system can provide uniform

traction from 0.01m/s to 0.3m/s. The whole driving circuit is shown in Fig. 2 (b).



(a) The experimental platform



(b) The platform-driven equipment

Fig. 2 The slide rail and its driving equipment used in the experiment

The whole system is placed in a laboratory tank. The tank has a length of 2.8 meters, width of 1.8 meters and depth of 1.0 meter. The robot is immersed in water with its center located at 0.1 meters below the surface of the water.

### B. Data Acquisition

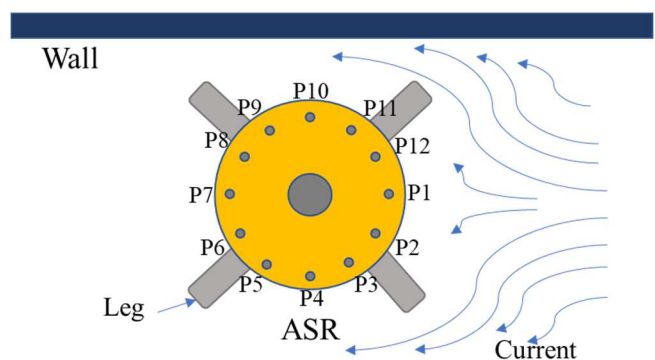


Fig. 3 The experimental scene and sensor distribution (P1-P12).

In order to realize the robot's perception of underwater obstacles (i.e. wall surface), a sensor system is arranged around the robot. The sensor system consists of high-precision pressure

sensor MS5803-01BA, which is evenly distributed 2cm away from the lower edge of the spherical body of the robot, as shown in Fig. 1.

The sensor system consists of 12 pressure sensors, whose distribution under water flow is shown in Fig. 3. The sensor is connected to the robot control panel through the chip selection and IIC interface. The control panel will process the collected data and judge the obstacles (wall surface).

In the experiment, 12 channels of pressure value data were introduced successively and in turn, and the sampling time of each channel was 0.1s.

### III. SIMULATION DATA AND RECOGNITION ALGORITHM

#### A. Simulation Data Acquisition

In addition, in order to further obtain more data, a simulation platform is built. The Lattice Boltzmann method is used to simulate the dynamic motion of the robot in a long pool. The length of the pool is 6.5 meters, the width is 2 meters, and the height is 2 meters. The length of the pool ensures the stability and data volume of the pressure sensor sampling.

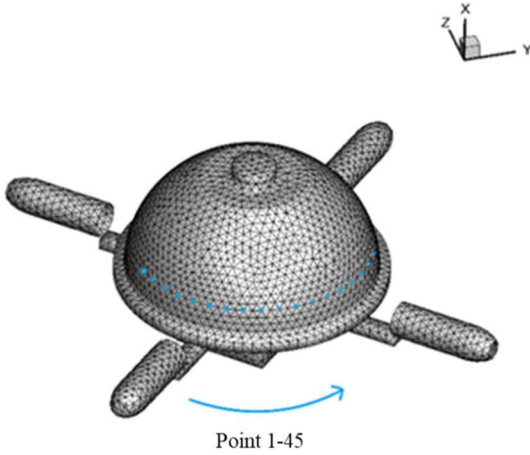


Fig. 4 The schematic diagram of sensor system on robot.

The sensor system is mainly composed of 90 pressure sensors densely arranged horizontally, as shown in Fig. 4. The 90 pressure sensors contain all the flow information around the robot and the flow conduction obstacle information. In the simulation, the dense pressure sensors are set up in order to understand the pressure sensing ability of the robot more comprehensively. It also provides a reference for optimizing the layout of sensors.

#### B. Verification of Simulation Data

In order to prove the validity of simulation data, simulation data and experimental data are compared under the same conditions. The robot is located in the centre of the pool, 0.9 meters away from the wall. Progress along the track at a speed of 0.1m/s in a 2.8m pool. Pressure perception data of experiment and simulation were collected, as shown in Fig. 5. It can be seen that the experimental data is similar to the simulation data.

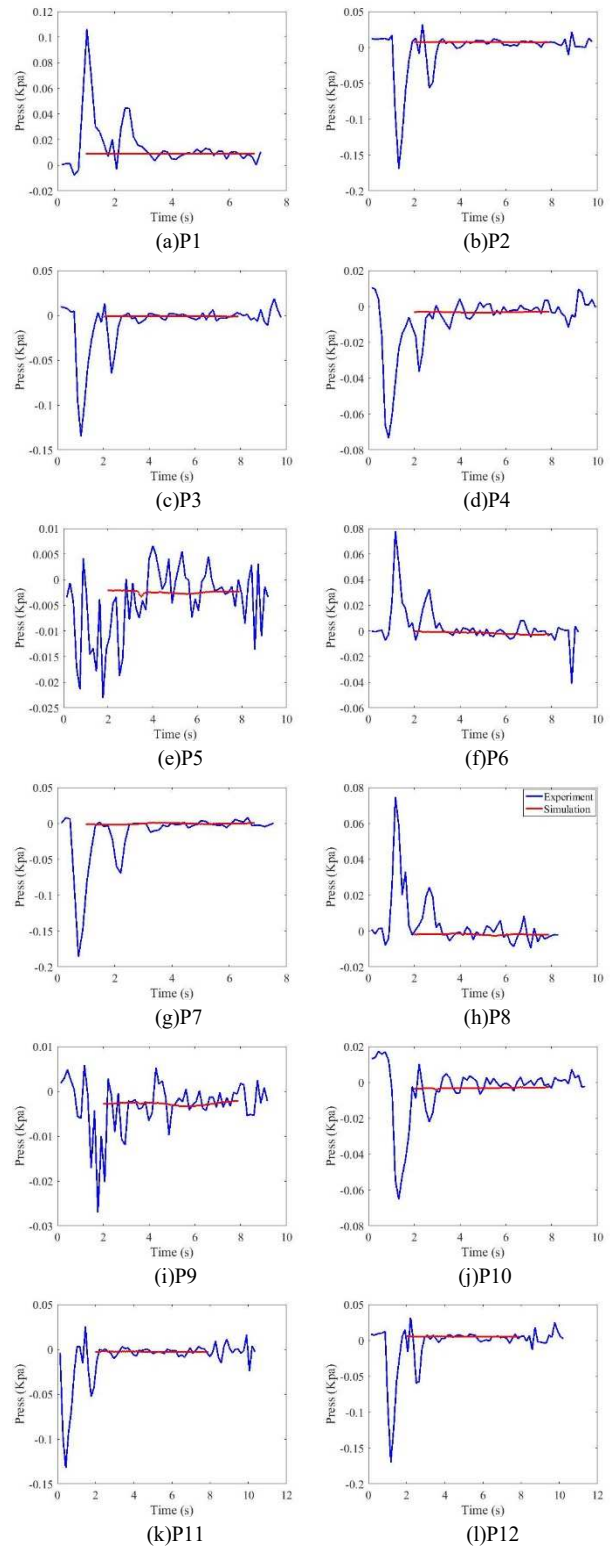


Fig. 5 The comparison of experimental results and simulation results.

The experimental results show that the simulation data can be used to analyse the pressure characteristics of the static obstacle.

#### C. Obstacle Recognition Algorithm

In order to simplify the calculation process, polynomials are often used to fit experimental data in practical applications. Pressure information and obstacle information from experimental data and simulation data will be related by polynomial regression. This polynomial can be used to recognize the position of obstacles in experiments.

Under a certain moving speed of the robot, the position of the obstacle and the value of pressure value perceived by the sensor are assumed to have the following functional relationship.

$$D = f(p, x) \quad (1)$$

$D$  represents the distance between the robot and an obstacle (such as a wall), and  $p$  represents the perceived pressure at the effective position  $x$  of pressure sensors on the robot. Function  $f(p, x)$  can be expanded to a polynomial in  $p$  and  $x$  according to Taylor's formula.

Take  $N$  data samples  $(p_i, x_i)$ ,  $i = 1, 2, \dots, N$ , the regression formula fitting the  $k$ -order polynomial can be expressed as:

$$D = a_0 + a_{11}x + a_{12}p + a_{21}x^2 + a_{22}p^2 + a_{23}xp + \dots \quad (2)$$

Root Mean Square Error (RMSE) is a measurement of the deviation between the observed value and the real value, and is often used as a standard to measure the prediction results of machine learning models. In practical measurements, the number of observations  $N$  is always finite, and the truth value can only be substituted by the most reliable value. When a quantity is measured more than once, the root mean square of the measurement error is taken. The smaller the value of root mean square, the better the fitting effect. The calculation method is as follows:

$$RMSE(p, x) = \sqrt{\frac{1}{N} \sum_{i=1}^N [\hat{D}(p, x) - D(p, x)]^2} \quad (3)$$

$\hat{D}(p, x)$  represents the predicted result and  $D(p, x)$  represents the real value.

#### IV. EXPERIMENT RESULTS AND DISCUSSIONS

In this part, firstly, the surface pressure characteristics of the underwater robot in the process of moving close to the obstacle (wall) are analyzed. Then the relationship between the distance between the robot and the obstacle, the pressure, and the sensor position is obtained by polynomial regression. Finally, the distance between the robot and the wall was predicted through simulation data and experimental data to analyzed the feasibility of our algorithm.

##### A. Robot Surface Pressure Characteristics

The robot moves in the channel at a speed of 0.1m/s. Fig. 6 shows the velocity distribution of the flow field during the robot movement. Fig. 6 (a) shows the flow field when the robot is almost close to the wall (0.221m from the center to the wall), Fig. 6.(b) shows the flow field when the center of the robot is 0.43m from the wall, and Fig. 6 (c) shows the robot at the center of the channel (0.85m from the center of the robot to the wall).

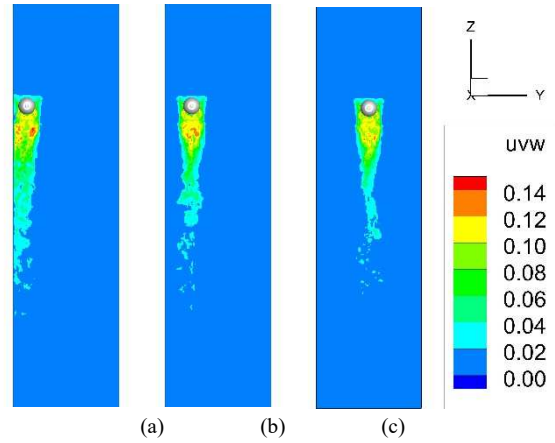


Fig. 6 Pressure distribution of robot surface at different distances from wall surface. (a) The robot is located in the center of the channel; (b) The robot is located 0.43m away from the wall; (c) The robot is located 0.221m away from the wall.

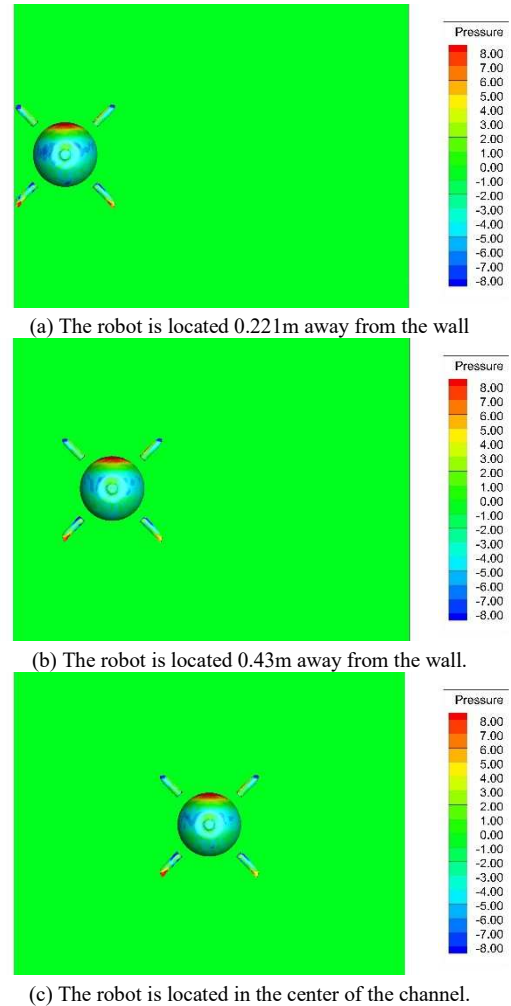
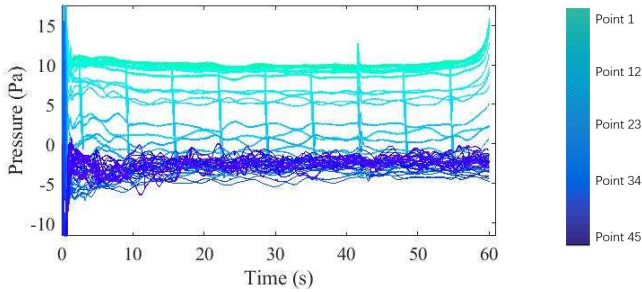


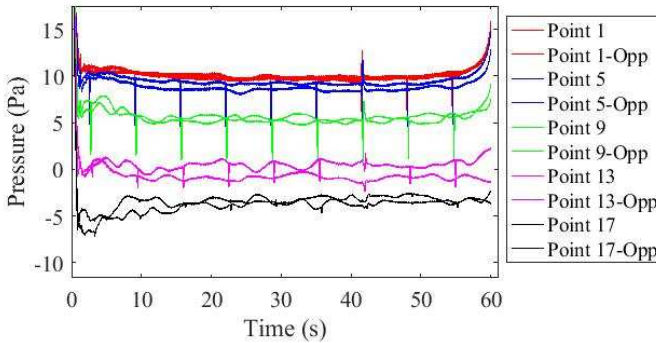
Fig. 7 Pressure distribution of robot surface at different distances from wall surface.

It can be seen that the wall surface has an effect on the flow field of the robot from Fig. 6. The closer the robot is to the wall,

the greater its motion fluctuation. In addition, the wall surface will also affect and attract the robot's wake.



(a) The pressure on the bottom edge of the hemispherical robot (The curve colors from light to dark represents the sensor from head to tail)



(b) The selected effective pressure  
Fig. 8 The pressure at the sampling points

Subsequently, we drew the surface pressure distribution of the robot corresponding to Fig. 6, as shown in Fig. 7. Fig. 7(a) shows the pressure distribution when the robot is almost close to the wall (0.221m from the center to the wall), Fig. 7.(b) shows the pressure distribution when the center of the robot is 0.43m from the wall, and Fig. 7 (c) shows the surface pressure of robot at the center of the channel (0.85m from the center of the robot to the wall). The pressure value was standardized according to the average underwater density, and the standardized result  $P$  was obtained, which was shown in Fig. 7.

It can be seen that as the distance from the wall decreases, the pressure distribution on the surface of the robot gradually becomes uneven, and the left and right pressure distribution are no longer symmetrical.

Then, the case is selected when the robot is 0.221m away from the wall surface. The pressure value of the robot around the bottom of the hemispherical ball is drawn, as shown in Fig. 8(a). The pressure on the vertical axis is normalized by static pressure at infinite distance. The colors from light to dark show the pressure values from the head to the tail of the robot to meet the flow. It can be seen that the pressure value of the robot head fluctuates little, which is suitable to be used as the feature of obstacle prediction.

In addition, the pressure of the robot tail fluctuates greatly and is unstable. This is due to the disturbance of tail turbulence during robot movement. Therefore, we choose the symmetrical sensor of the robot head part as the basis for obstacle

recognition. Fig. 8 (b) shows the pressure variation values of some points on the head of robot and their symmetric points.

### B. Recognition Accuracy

According to the analysis in the above section, the pressure difference between the two sides of the robot can represent the pressure characteristics when the robot is close to the wall. In polynomial regression, the difference of pressure values on bilateral symmetry of the robot is used as  $p$  input. Sensor placement points are selected from the robot head with prominent features (from 1 to 8). These points are labeled  $x$  in polynomial regression. The distance from the wall is the predicted quantity  $D$ . In order to facilitate calculation, all variables  $p$ ,  $x$  and  $D$  are normalized to the interval  $[-0.5, 0.5]$ . And then we do second-order polynomial regression. The regression model is assumed to be:

$$D = a_0 + a_{11}x + a_{12}p + a_{21}x^2 + a_{22}p^2 + a_{23}xp \quad (4)$$

Through the regression algorithm, the corresponding coefficients of the polynomial are obtained, as shown in Table 1. Fig. 9 shows the regression surface and sampling points. It can be seen that the regression surface fits the sampling points well.

TABLE I  
THE SECOND-ORDER POLYNOMIAL REGRESSION PARAMETER VALUES

Parameter	Value	Parameter	Value
$a_0$	0.15267994	$a_{21}$	2.01990463
$a_{11}$	-1.85843478	$a_{22}$	0.14216714
$a_{12}$	-2.23202503	$a_{23}$	2.93965213

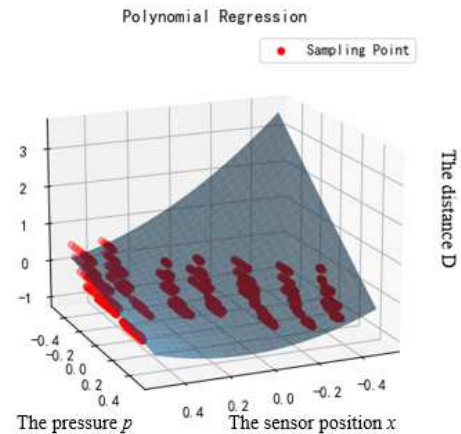


Fig. 9 The second order polynomial regression fitting surface and sampling point

The average error obtained by fitting 1575 sampling points is 0.189832. The fitting results are within the acceptable error range. In order to further improve the fitting accuracy, a third order polynomial model is established. The third-order polynomial is shown in formula 5.

The third-order polynomial is fitted and its coefficients are shown in Table 2. The fitting surfaces and sampling points are shown in Fig. 10.

$$D = a_0 + a_{11}x + a_{12}p + a_{21}x^2 + a_{22}p^2 + a_{23}xp + a_{31}x^3 + a_{32}p^3 + a_{33}x^2p + a_{34}xp^2 \quad (5)$$

TABLE II  
THE THIRD-ORDER POLYNOMIAL REGRESSION PARAMETER VALUES

Parameter	Value	Parameter	Value
$a_0$	0.25385269	$a_{23}$	5.83977109
$a_{11}$	-3.22892112	$a_{31}$	2.61518414
$a_{12}$	-2.80766451	$a_{32}$	3.55348444
$a_{21}$	3.06678921	$a_{33}$	-6.16690217
$a_{22}$	0.48142837	$a_{34}$	1.77806528

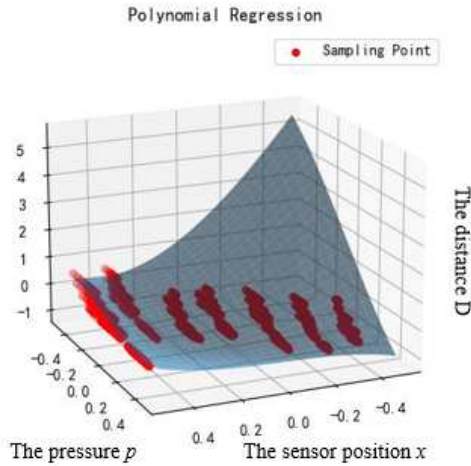


Fig. 10 The third order polynomial regression fitting surface and sampling point

Through the same sampled data, the average error obtained by third-order polynomial regression is 0.164652. It can be seen that increasing the order of polynomial regression has a certain effect on reducing the error, and the error is also within the acceptable range of the prediction.

#### IV. CONCLUSION

This paper explores the recognition of static obstacles through the artificial lateral line system established by the pressure sensor. Firstly, the underwater pressure characteristics of an underwater moving robot near a static obstacle (such as a wall) are analyzed by simulation and experiment. Based on the analysis of pressure characteristics, the principle and feasibility of sensing static obstacles are obtained. Then a polynomial regression model is established to analyze a large number of sampling points. The second and third order regression models can predict the distance between the robot and the wall well. This paper presents a new idea and scheme in static obstacle recognition.

#### REFERENCES

- [1] C. Li and S. Guo, "Adaptive Multi-Mode Switching Strategy for the Spherical Underwater Robot with Hybrid Thruster," *Advanced Engineering Informatics*, vol. 55, pp. 101845, Jan 2022.
- [2] R. An, S. Guo and Y. Yu, "Task Planning and Collaboration of Jellyfish-inspired Multiple Spherical Underwater Robots," *Journal of Bionic Engineering*, vol. 19, no. 3, pp. 643-656, May 2022.
- [3] L. Zacchini, A. Topini and M. Franchi, "Autonomous Underwater Environment Perceiving and Modeling: An Experimental Campaign With FeelHippo AUV for Forward Looking Sonar-Based Automatic Target Recognition and Data Association," *IEEE Journal of Oceanic Engineering*, vol. 48, no. 2, pp. 277-296, Nov 2022.
- [4] KB. Xie, J. Yang and K. Qiu, "A Dataset with Multibeam Forward-Looking Sonar for Underwater Object Detection," *Scientific Data*, vol. 9, no. 1, pp. 739, Dec 2022.
- [5] YG. Jiang, Z. Gong and Z. Yang, "Underwater Source Localization Using an Artificial Lateral Line System With Pressure and Flow Velocity Sensor Fusion," *IEEE-ASME Transactions on Mechatronics*, vol. 27, no. 1, pp. 245-255, Feb 2022.
- [6] A. Garcia-Vega, JF. Fuentes-Perez and S. Fukuda, "Artificial lateral line for aquatic habitat modelling: An example for *Lefua echigonia*," *Ecological Informatics*, vol. 65, pp. 101388, Aug 2021.
- [7] X. Zheng, W. Wang and L. Li, "Artificial lateral line based relative state estimation between an upstream oscillating fin and a downstream robotic fish," *Bioinspiration & Biomimetics*, vol. 16, no. 1, pp. 016012, Jan 2021.
- [8] J. Zheng, X. Zheng and T. Zhang, "Dual-sensor fusion based attitude holding of a fin-actuated robotic fish" *Bioinspiration & Biomimetics*, vol. 15, no. 4, pp. 046003, Jul 2020.
- [9] MM. Wang, B. Jin and GJ. Liu, "The moving vibration source perception using bionic lateral line system and data-driven method," *Ocean Engineering*, vol. 247, pp. 110463, Feb. 2022.
- [10] YG. Jiang, Z. Gong and Z. Yang, "Underwater source localization using an artificial lateral line system with pressure and flow velocity sensor fusion," *IEEE-ASME Transactions on Mechatronics*, vol. 27, no. 1, pp. 245-255, Feb 2022.
- [11] T. Jeong, J. Yoo and D. Kim, "Deep learning model inspired by lateral line system for underwater object detection," *Bioinspiration & Biomimetics*, vol. 17, no. 2, pp. 026002, Mar. 2022.
- [12] X. Zheng, Y. Zhang, GJ. Liu, "Underwater positioning based on an artificial lateral line and a generalized regression neural network," *Journal of Bionic Engineering*, vol. 15, no. 5, pp. 883-893, Sep. 2018
- [13] D. Xu, Y. Zhang and J. Tian, "Optimal sensor placement of the artificial lateral line for flow parametric identification Sensors," *Sensors*, vol. 21, no. 12, pp. 3980, Jun. 2021.
- [14] C. Li and S. Guo, "Characteristic Evaluation via Multi-Sensor Information Fusion Strategy for Spherical Underwater Robots," *Information Fusion*, vol. 95, pp. 199-214, 2023.
- [15] S. Gu, S. Guo, L. Zheng and R. An, "Communication and Cooperation for Spherical Underwater Robots by Using Acoustic Transmission," *IEEE-ASME Transactions on Mechatronics*, Feb. 2022.
- [16] C. Li, S. Guo and J. Guo, "Study on Obstacle Avoidance Strategy Using Multiple Ultrasonic Sensors for Spherical Underwater Robots," *IEEE Sensors Journal*, vol. 22, no. 24, pp. 24458-24470, Dec. 2022.
- [17] R. An, S. Guo and L. Zheng, "Uncertain moving obstacles avoiding method in 3D arbitrary path planning for a spherical underwater robot," *Robotics and Autonomous Systems*, vol.151, pp. 104011, May. 2022.
- [18] A. Li, S. Guo, M. Liu and H. Yin, "Hydrodynamic Characteristics-based Adaptive Model Predictive Control for the Spherical Underwater Robot Under Ocean Current Disturbance," *Machines*, vol. 10, no. 9, pp. 798, Sep. 2022.
- [19] H. Yin, SX. Guo, M. Liu, "A Virtual Linkage-Based Dual Event-Triggered Formation Control Strategy for Multiple Amphibious Spherical Robots in Constrained Space With Limited Communication," *IEEE Sensors Journal*, vol. 22, no. 13, pp. 13395-13406, Jul. 2022.